JACS
JOURNAL OF THE AMERICAN CHEMICAL SOCIETY

Article

pubs.acs.org/JACS

Quantitative Analysis of Structure and Bandgap Changes in Graphene Oxide Nanoribbons during Thermal Annealing

Yu Zhu,[†,‡] Xianyu Li,[§] Qinjia Cai,[§] Zhengzong Sun,[†,‡] Gilberto Casillas,[⊥] Miguel Jose-Yacaman,[⊥] Rafael Verduzco,*[,§] and James M. Tour*[,†,‡,∥]

[†]Departments of Chemistry and the [‡]Smalley Institute for Nanoscale Science and Technology, Rice University, MS 222, 6100 Main Street, Houston, Texas 77005, United States

[§]Department of Chemical and Biomolecular Engineering, Rice University, MS 362, 6100 Main Street, Houston, Texas 77005, United States

[⊥]Department Physics and Astronomy, University of Texas at San Antonio, One UTSA Circle, San Antonio, Texas, 78249

[∥]Mechanical Engineering and Materials Science, Rice University, 6100 Main Street, Houston, Texas 77005, United States

Supporting Information

ABSTRACT: Graphene oxide nanoribbons (GONRs) are wide bandgap semiconductors that can be reduced to metallic graphene nanoribbons. The transformation of GONRs from their semiconductive to the metallic state by annealing has attracted significant interest due to its simplicity. However, the detailed process by which GONRs transform from wide-bandgap semiconductors to semimetals with a near zero bandgap is unclear. As a result, precise control of the bandgap between these two states is not currently achievable. Here, we quantitatively examine the removal of oxygen-containing groups and changes in the bandgap during thermal annealing of GONRs. X-ray photoelectron spectroscopy measurements show the progressive removal of oxygen-containing functional groups. Aberration-corrected scanning transmission electron microscopy reveals that initially small graphene regions in GONRs become large stacked graphitic layers during thermal annealing. These structural and chemical changes are correlated with progressive changes in the electrochemical bandgap, monitored by cyclic voltammetry. These results show that small changes in the thermal annealing temperature result in significant changes to the bandgap and chemical composition of GONRs and provide a straightforward method for tuning the bandgap in oxidized graphene structures.

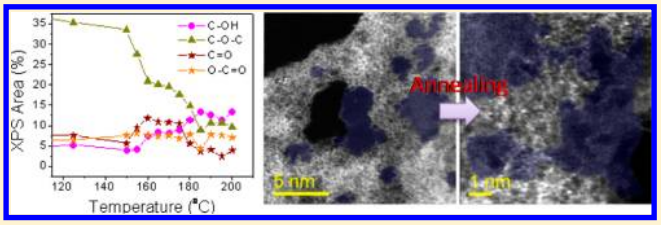

INTRODUCTION

Graphene nanoribbons (GNRs) are narrow, elongated strips of graphene with a bandgap dependent on their widths. As the GNR width increases, the bandgap decreases, and GNRs evolve from a semiconductor to a semi-metal. Narrow GNRs (width <10 nm) can have band gaps that are affected by edge configurations; however, such narrow structures are not considered here.[1−11] Various techniques have been proposed for generating ribbon-like graphene with a substantial bandgap,[12−15] but no method exists for producing bulk quantities of semiconductive GNRs. By contrast, graphene oxide nanoribbons (GONRs) can be produced through the longitudinal unzipping of carbon nanotubes, a scalable, solution-based synthetic procedure.[8,10] The resulting GONRs have large bandgaps (~4 eV)[16−20] due to the distorted structures originating from oxygen-containing substituents; however, by chemical reduction or thermal annealing, oxygen-containing functional groups can be removed, transforming semiconductive GONRs to semimetallic GNRs. GONRs and their reduced products are therefore attractive materials for flexible thin film electronics due to their adjustable bandgap and scalable preparation methods.[7,11] Access to a solution-processable form of graphene with a tunable bandgap would be of particular interest for numerous applications including organic photovoltaics, transistors, and sensors.

The bandgap of GONRs progressively decreases from 2 to 4 eV to nearly 0 eV under thermal annealing or chemical reduction.[8,10,17,18,21−24] Semiconductive states of GONRs[23,24] and semimetallic states of reduced GONRs[8,10] have also been reported. Nevertheless, the process by which GONRs transform between two extreme states has not been detailed, which makes accurate control of the bandgap difficult and limits their applications. Furthermore, detailing the changes of GONR under thermal annealing may provide clues for understanding the large differences among reported bandgaps of graphene oxide (GO, a GONR analogue with an aspect ratio ~1).[16−18,21,22,25−28] Here, we systematically investigate the structural, chemical, and electronic changes of thermally annealed GONRs using a combination of X-ray photoelectron spectroscopy (XPS), cyclic voltammetry (CV), and aberration-corrected scanning transmission electron microscopy (STEM).

Received: May 8, 2012
Published: June 21, 2012

   dx.doi.org/10.1021/ja304471x | J. Am. Chem. Soc. 2012, 134, 11774−11780

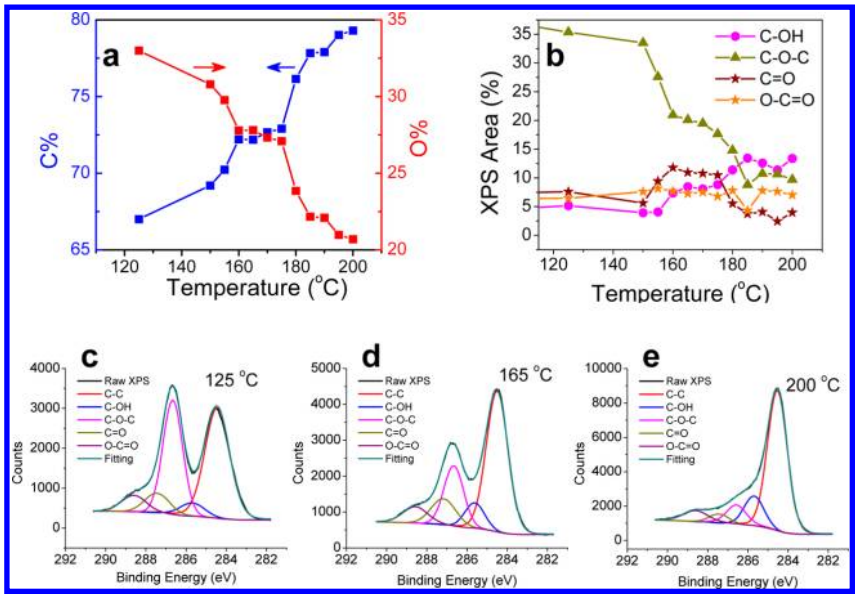

Figure 1. XPS data on the evolution of carbon and oxygen content in GONR during annealing. (a) Carbon and oxygen concentrations in GONRs. The survey scan of the XPS shows carbon and oxygen are the major content in all GONR films. The concentration of the two elements are calculated on the basis of the high-resolution XPS scan of carbon C1s signal and oxygen C1s signal. (b) XPS area percentage change of oxygen-containing groups based on the peak fitting results. (c–e) Fitting results of high-resolution XPS C1s signals for GONRs films annealed at 125, 165, and 200 °C, respectively.

XPS reveals the progressive removal of oxygen-containing functionalities during thermal annealing. The CV[29,30] of thermally annealed GONRs provides a measure of the electrochemical bandgap, and we find that GONRs remain semiconductive at low annealing temperatures but transition to semimetals at higher annealing temperatures, consistent with the XPS results. STEM provides direct evidence for the growth of graphene regions in the annealed GONRs from initially isolated graphene islands. Taken together, these results show that small changes in the thermal annealing temperature result in significant changes to the bandgap and chemical composition of GONRs and provide a straightforward method for tuning the bandgap in oxidized graphene structures.

EXPERIMENTAL SECTION

GONRs were prepared by using the previously reported carbon nanotube unzipping technique where multiwalled carbon nanotubes were treated with potassium permanganate in acid.[8,10] The GONRs were dispersed in water to form a solution with a concentration of 0.1 mg/mL. The thin film samples were prepared by drop-casting the GONR solutions onto various substrates. The cast films were air-dried and kept in a desicator in a glovebox overnight. Thermal annealing was carried out using a preheated digital hot plate in the glovebox. The annealing time was 10 min for all samples, which ensures that the films reached the specified annealing temperatures. Specifically, the annealing temperatures tested included 125 and 150 °C, and then temperatures from 150 to 200 °C in 5 °C increments.

XPS was carried out on a PHI Quantera SXM Scanning X-ray Microprobe with a base pressure of 5×10^{-9} Torr. As an X-ray source, an Al cathode at 40 W was used with a pass energy of 26.00 eV, 45° takeoff angle, and a 200 μm beam size. Low-resolution survey scans as well as high-resolution scans of C and O were taken. C1s spectra were shifted to standard positions (284.5 eV).

The XPS program Multipak v9.0 from ULVAC-PHI, Inc. was used for fitting. The initial chemical shifts of the C–C bond, C–OH bond, epoxide, C═O bond, and O–C═O bond were set to 284.5, 285.75, 286.6, 287.3, and 288.5 eV, respectively. A tolerance of ±0.1 eV (±0.25 eV for the C–OH bond) shift from the initial peak position was allowed during the fitting. The full-width half-maximum (fwhm) of all five peaks were kept within a difference of 0.3 eV during fitting. The fitting was carried out by a Lorentz–Gauss algorithm.

For CV experiments, thin films of the annealed GONRs were prepared on a gold electrode and cycled in degassed, anhydrous acetonitrile containing 0.1 M tetrabutylammonium hexafluorophosphate as the electrolyte. The counter and reference electrodes were platinum. The voltage data were corrected using ferrocene; the scan rate was 100 mV/s, and the temperature was 20 °C. For each annealing temperature, 3–5 samples were measured. The oxidation and reduction cycles were performed with fresh films and fresh electrolyte, which avoids conflation of the results due to the irreversible change of the GONRs after the redox cycles. The oxidation onset potential and reduction onset potential were recorded, which were then used to calculate the energies of highest occupied molecular orbital (HOMO) and lowest unoccupied molecular orbital (LUMO) of the GONRs. The bandgaps of the GONRs at different annealing temperatures were calculated using the HOMO and LUMO information.

Atomic resolution STEM images were taken using a JEOL ARM200F operated at 80 kV equipped with spherical aberration probe corrector. The sample was prepared by drop-casting a GONRs solution on a QUANTIFOIL substrate having orthogonal array of 1.2-μm diameter holes with ~1.3-μm separation and mounted on a 200-mesh gold grid. The samples were dried in vacuum for 24 h before use. Only the sample without annealing and the sample annealed at 200 °C were studied by STEM. Annealing was carried out in a glovebox, and the TEM grid with the drop-casted GONR samples was baked at 200 °C for 10 min. Then the samples were transferred to the STEM chamber and were beam-showered for 10 min to decrease the charging effect.

RESULTS AND DISCUSSION

XPS measurements provided information on chemical changes occurring in GONR films during annealing. GONRs were drop-casted in aqueous solution onto a silicon substrate (p-Si substrates with 500 nm thermal oxide) and thermally annealed using a hot-plate in a glovebox at temperatures ranging from 125 up to 200 °C. High-resolution XPS C1s and O1s spectra were collected, and the ratio of the two elements was calculated. The XPS results are shown in Figure 1 and

dx.doi.org/10.1021/ja304471x | J. Am. Chem. Soc. 2012, 134, 11774–11780

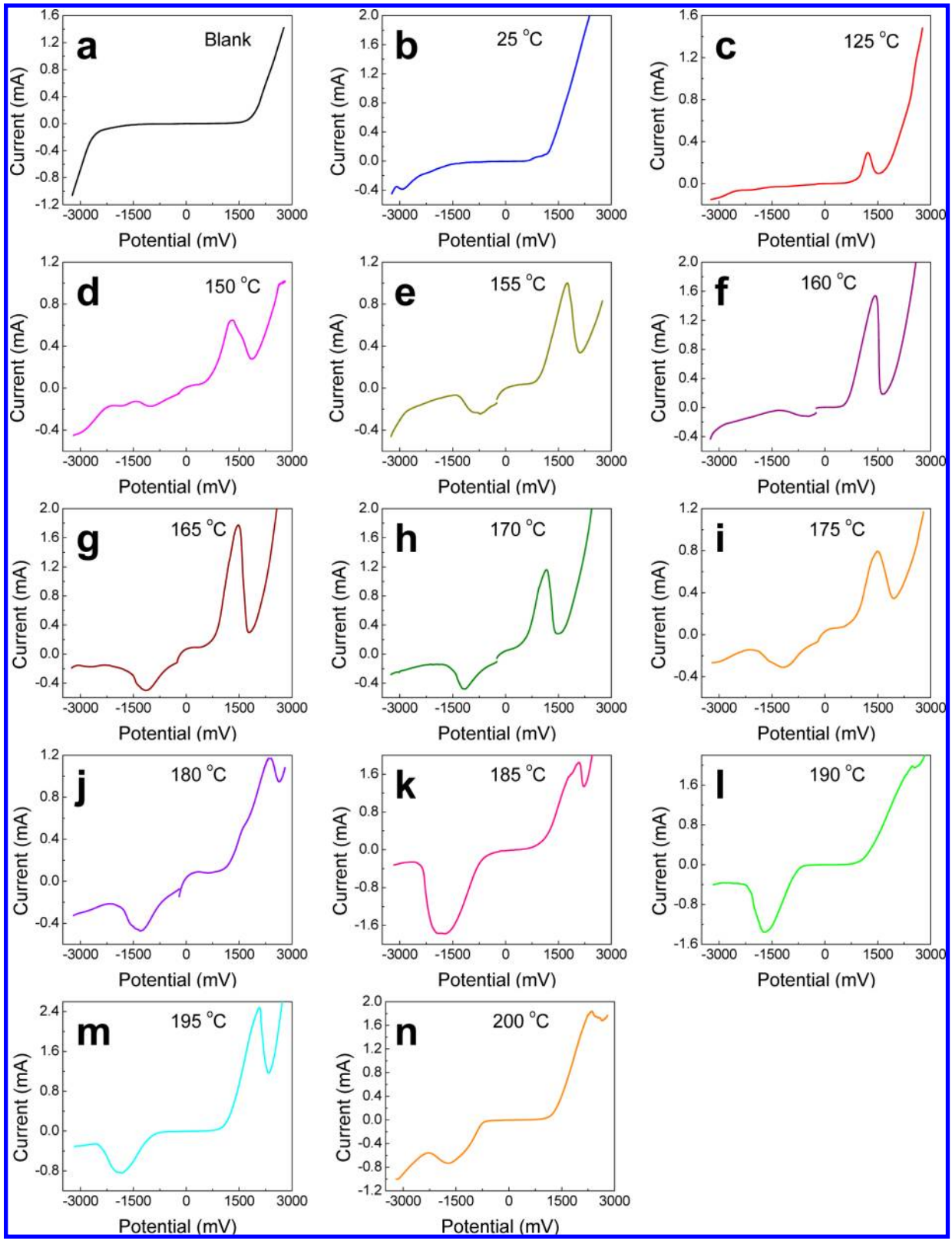

Figure 2. Cyclic voltammetry of GONRs films. (a) Blank test using a gold working electrode with no GONR film on it. (b) CV of a nonannealed GONR film. (c–n) CV of GONR films annealed at the indicated temperature. CV measurements were carried out in degassed, anhydrous acetonitrile containing 0.1 M tetrabutylammonium hexafluorophosphate as the electrolyte. Counter and reference electrodes are platinum. The working electrode is gold. The scan rate is 100 mV/s at a temperature of 20 °C. The oxidation and reduction cycle are performed separately with fresh film and electrolyte. The experiments are carried out with reverse scans for both oxidation and reduction processes, but only forward scans of oxidation and reduction are presented for clarity. The oxidation and reduction onset potentials are deduced from the forward scans. All potentials are calibrated using a ferrocene standard.

dx.doi.org/10.1021/ja304471x | J. Am. Chem. Soc. 2012, 134, 11774–11780

Supporting Information Figure S1−S2. With increasing annealing temperatures, XPS measurements show a decreasing content of oxygen along with an increase in the content of carbon (Figure 1a). Interestingly, the oxygen concentration is roughly a constant at annealing temperatures between 160 and 175 °C.

To determine the functional groups present in the thermally annealed GONR samples, XPS C1s spectra were fit to a Lorentz−Gauss algorithm for various chemical functionalities: C−C bond, C−OH bond (hydroxyl), C−O−C (epoxide), C═O bond (carbonyl), and O−C═O bond (carboxylic acid).[8,10,18,21,25−27,31] Shifting the C−C bond signal of all the C1s spectra to 284.5 eV (aromatic) enables quantitative comparison between the various C1s spectra. Note that the XPS binding energy for C−C bonds may be shifted to different values in the literature; however, the relative shift in the binding energy of various carbon−oxygen functionalities is nearly constant in most examples. On the basis of previous reports,[10,32] we adopt the following chemical shifts relative to C−C bonds: 1.0−1.5 eV for C−OH bond, 2.0−2.2 eV for epoxide, 2.7−2.9 eV for C═O bond and 3.9−4.1 eV for O−C═O bond. The signals at 284.5, 285.5−286, 286.5−286.7, 287.2−287.4, and 288.4−288.6 eV are therefore assigned to the C−C bond, C−OH bond, C−O−C bond, C═O bond, and O−C═O bond, respectively. In the fitting program, the chemical shifts of various carbon bonds were set to the middle value of the above range and the range restriction for each bond was applied during the fitting. The fwhm's of all five peaks were also kept within a difference of 0.3 eV during fitting. More detailed information on the fitting procedure is provided in the Experimental Section. Fitting results are shown in Figure 1c−e for annealing at 125, 165, and 200 °C, respectively (additional annealing temperatures are provided in the Supporting Information Figure S1). The model provides a good match to the original spectra, and the fwhm for different carbon bond signals are similar, indicating the physical existence of all proposed carbon bonds.

The evolution of oxygen-containing groups is qualitatively presented in Figure 1b and Figure S2 in Supporting Information. The results indicate that epoxide functionalities represent the majority of oxygen-containing groups on as-prepared GONRs and that the concentration of epoxides progressively decreases with increasing annealing temperature. In contrast, the concentration of hydroxyl functionalities increases during annealing, and the carbonyl group content increases with annealing over a temperature range from 125 to 160 °C, and then remains unchanged between 160 and 175 °C, and then sharply decreases for annealing temperatures greater than 180 °C. These trends can be explained by the different stabilities of the various functional groups. The epoxide groups are least stable and continuously decrease with increasing annealing temperature, and the broad range over which epoxide functionalities are lost may reflect the presence of different chemical environments around the epoxide groups. The increase in hydroxyl groups at low annealing temperatures reflects the partial decomposition of epoxide groups to produce hydroxyl groups. This hypothesis is consistent with the observed two-step increase in the hydroxyl group content coincident with a decrease of epoxide groups (Figure 1b). In the case of carbonyl groups, the initial increase may be due to the decomposition of epoxide groups. From 160 and 175 °C, the carbonyl group content remains unchanged, similar to epoxide group and hydroxyl group contents. The decrease of the carbonyl group content at temperatures higher than 180 °C indicates decomposition of the carbon═oxygen double bond. Finally, due to the stability of carboxylic acid groups, their content is almost unchanged during the annealing. Overall, XPS indicates a loss of oxygen-containing groups during thermal annealing, which can be correlated to a more planar graphene structure with greater sp^2-carbon character. This is confirmed by the smaller fwhm of the C−C bond from Figure 1c to 1e.

As-prepared GONRs are highly oxidized and contain various oxygen functionalities on the edge and basal surface of the ribbons.[8,10] These attached functional groups are known to distort the planar structure of graphene, resulting in a bandgap greater than 3 eV. As the oxygen functionalities are removed, the bandgap should decrease due to a more planar graphene structure. To investigate changes in the electronic bandgap, CV measurements were carried out on thermally annealed samples. The GONR films were cast on gold electrodes and annealed at different temperatures (Figure 2) for 10 min. For clarity, only forward scans are presented in Figure 2. For each measurement, the onset potential can be determined from the intersection of two tangents drawn at the rising and background current of the CV, as listed in Table 1.

Table 1. Onset Potentials and Bandgap Information of GONRs Film Based on CV Experiments

annealing temperature (°C)	oxidation onset (V)	reduction onset (V)	HOMO (eV)[a]	LUMO (eV)[a]	bandgap (eV)
25	1.27	−2.46	−6.07	−2.34	3.73
125	0.96	−2.45	−5.76	−2.35	3.41
150	0.75	−0.76	−5.55	−4.04	1.51
155	0.96	−0.24	−5.76	−4.56	1.18
160	0.68	−0.15	−5.48	−4.65	0.83
165	0.84	−0.24	−5.64	−4.56	1.08
170	0.64	−0.41	−5.44	−4.39	1.05
175	0.88	−0.18	−5.68	−4.62	1.06
180	1.19	−0.40	−5.99	−4.40	1.59[b]
185	1.16	−0.70	−5.96	−4.10	1.89[b]
190	1.16	−0.76	−5.96	−4.04	1.92[b]
195	1.18	−0.99	−5.98	−3.81	2.17[b]
200	1.34	−0.76	−6.14	−4.04	2.10[b]

[a]The HOMO−LUMO gaps were calculated according to the equation: $-E_{LUMO} = E_{onset(red)} + 4.8$ eV and $-E_{HOMO} = E_{onset(ox)} + 4.8$ eV, where $E_{onset(ox)}$ and $E_{onset(red)}$ are the onset potentials for the oxidation and reduction processes, respectively, of GONRs films vs ferrocene/ferrocene$^+$. [b]Contains a mixture of semiconductive and semimetallic domains

Nonannealed GONR films show a reduction peak around −2.9 V, but the oxidation peak is out of the measurable range. Based on the onset potentials for oxidation and reduction, 1.27 V and −2.46 V, respectively, the bandgap for nonannealed GONRs is 3.7 eV, similar to the reported bandgap of GO.[17,33] CV measurements show that the bandgap decreases to ∼1 eV as the annealing temperature is increased from room temperature to 160 °C (Table 1). Furthermore, annealing at temperatures from 160 to 175 °C does not further decrease the bandgap. Surprisingly, at annealing temperatures above 180 °C, CV measurements show an increase in the bandgap. This is unexpected since progressive removal of oxygen containing functionalities should result in a further bandgap decrease, which is caused by the increase of sp^2 carbon structure size on the GONRs. However, this may be attributed to the emergence

dx.doi.org/10.1021/ja304471x | J. Am. Chem. Soc. 2012, 134, 11774−11780

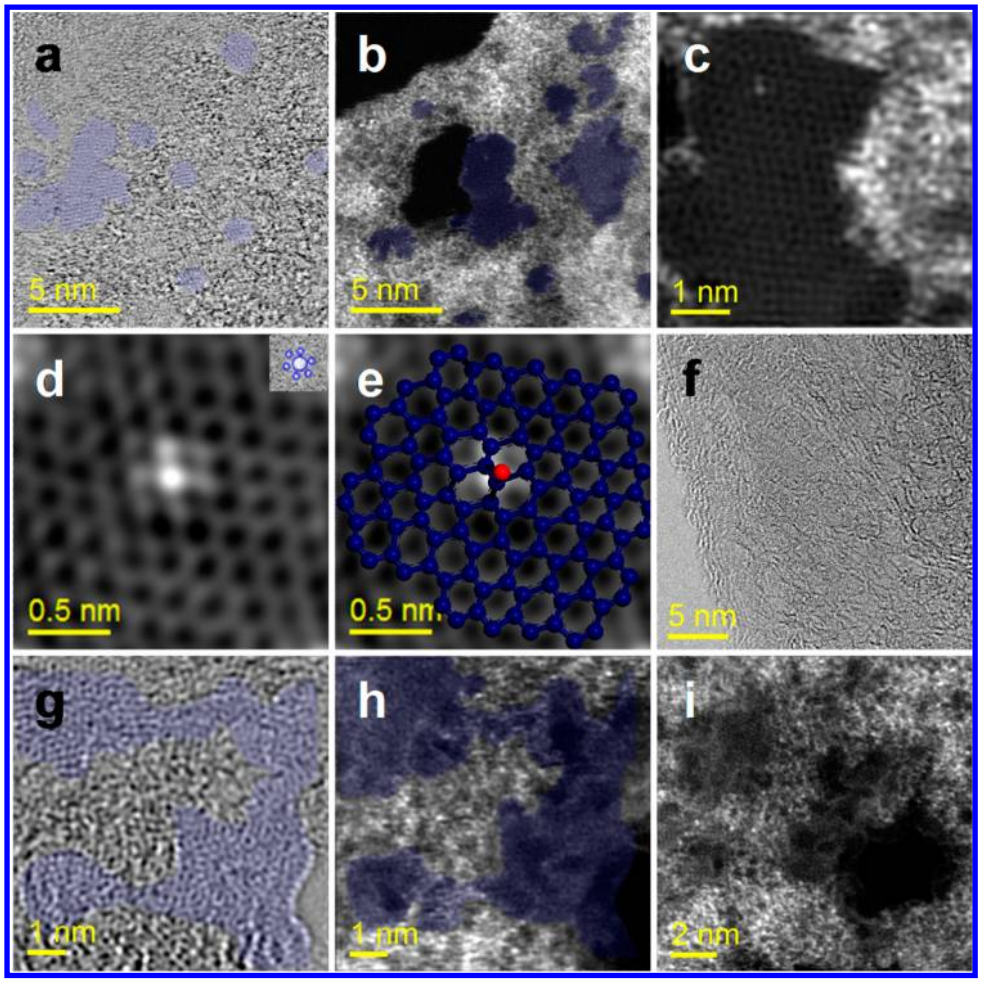

Figure 3. STEM images of the GONRs ribbons. (a–e) Nonannealed GONRs and (f–i) GONRs annealed at 200 °C for 10 min. (a) Bright field (BF) STEM image of GONRs ribbons with graphene regions shown in blue. (b) High-angle annular dark-field (HAADF) STEM image of GONRs ribbons with graphene regions shown in blue. (c) HAADF STEM image of a monolayer graphene region (same area as the center in Figure 3b). (d) High-resolution image of monolayer graphene with an oxygen functional group on the basal surface after applying a filter (upper-right inset) to the FFT of the raw HAADF STEM image. (e) HAADF STEM image of the same region shown in Figure 3d with an overlay structure sketch. (f) BF STEM image of annealed GONRs with stacked graphene layers. (g) BF STEM image of annealed GONRs with graphene regions shown in blue. (h) HAADF STEM image of annealed GONRs graphene regions shown in blue. (i) HAADF STEM image of annealed GONRs with holes. A band-pass filter was applied in (a–c) and (g–i) to decrease the noise.[34].

of continuous metallic regions in the GONR film, which is further confirmed by STEM experiments as discussed below. As the GONRs change to a mixture of both semiconductive and metallic regions, the CV-measured electrochemical bandgap may experience a nonmonotonic change since the CV measurements only reflect electrochemical properties of the semiconductive GONR regions. The metallic regions act as electrodes and are not reflected in the bandgap measurement. Similar phenomena have been observed in CV measurements of carbon nanotubes, which contain both semiconductive and metallic nanotubes.[29] In Table 1, we designate by an asterisk those samples which exhibit an increased bandgap at high annealing temperatures and which we infer to contain a mixture of semiconductive and semimetallic domains.

By comparing CV and XPS results, we can correlate bandgap changes to cleavage of different chemical functionalities. During the first annealing phase, from 125 to 160 °C, the most easily cleaved groups (epoxide) are removed, and the bandgap of the GONRs decreases monotonically with temperature due to the regeneration of the sp^2-carbon structure of graphene. From 165 to 175 °C, no significant chemical changes occur, and therefore the bandgap of the annealed GONRs remains nearly unchanged. When the annealing temperature is above 180 °C, there is a further loss of functional groups, and this leads to the emergence of metallic graphene regions with extended sp^2-carbon structure. There is still a significant amount of oxygen in the material at this stage (oxygen concentration ~20%), and therefore the material becomes a mixture of metallic graphene and semiconductive oxygen-containing (mostly hydroxyl and carboxylic acid groups) functionalized regions.

The chemical changes described above are directly related to the GONR planarity and sp^2-carbon structure of GONRs which can be directly imaged by STEM. Only nonannealed GONR samples and samples annealed at 200 °C for 10 min were investigated by STEM. The use of an aberration-corrector enables the identification of atomic structure of GONRs. In the nonannealed samples (Figure 3a–e), nanoscale regions of monolayer graphene are observed. The sizes of the graphene regions are typically in the range of 1–2 nm, while in some directions it can be as long as 3–5 nm, as shown in a and b of Figure 3 (more STEM images are shown in Supporting Information Figures S3 and S4). However, the majority of the

dx.doi.org/10.1021/ja304471x | J. Am. Chem. Soc. 2012, 134, 11774–11780

film is functionalized with oxygen-containing groups, as indicated by the nonstained regions in Figure 3a,b, where they are sp^3-carbon rich. This indicates that graphitic regions are small and isolated in a nonannealed sample, as expected from the large bandgap (>3 eV) measured by CV.

The use of an aberration-corrector gives atomic detail of GONRs, and a single oxygen-containing functionality can be identified in a nanoscale region of graphene (d and e of Figure 3). Figure 3e shows the sketch based on the contrast-enhanced high-resolution HAADF STEM image. The position of the defect suggests the presence of an epoxy group; such groups are abundant on the nonannealed ribbon basal planes. The results agree well with the previous TEM simulations showing an epoxy group bridging the adjacent carbon atoms on a ring.[35] Additional images are shown in Supporting Information Figures S3 and S4.

After the sample was annealed at 200 °C for 10 min, STEM reveals regions of multilayer stacked graphene instead of the monolayer graphene originally seen before annealing (Figure 3f–i). As shown in image f of Figure 3, 4 to 5 graphene layers are stacked. Bright field image g in Figure 3 and dark field images h and i in Figure 3 show that there is no clear single-layer graphene region. The stacking of the graphene sheets suggests that out-of-plane functional groups are removed with annealing. Although the oxygen-containing functional groups are still present (the bright area in images h and i of Figure 3), the previously isolated graphitic regions on GONRs have been merged, as indicated by the blue-stained regions. With the likelihood of conductive paths between layers, annealed GONRs structures in f–i of Figure 3 can be estimated to have graphene/graphite regions greater than 10 nm in size. On the basis of the previous experimental and theoretical work,[5,6,19,20,36] the quantum confinement-induced bandgaps of graphene are found to be observable only when the size of the sp^2-carbon structure is small. The sp^2-carbon structure observed in Figure 3f–i (over 10 nm and multilayer stacked) is large, and the material should have small bandgaps (<100 meV or near 0 eV). These STEM measurements provide direct evidence that thermal annealing results in the emergence of metallic regions, and that the final GONR films contain a mixture of both semiconductive and semimetallic regions.

CONCLUSIONS

The combination of XPS, CV, and STEM analysis of annealed GONR provides a comprehensive picture of the evolution from the semiconductive to the semimetallic state. Semiconductive GONRs have large bandgap (>3 eV) and isolated sp^2-carbon structures smaller than 5 nm. Annealing at a relative low temperature (160–175 °C) leads to the decomposition of some epoxide groups, and the bandgap of GONRs decreases to about 1 eV. Annealing at higher temperatures (over 175 °C) results in the decomposition of more oxygen-containing groups (epoxide and carbonyl groups), which leads to the formation of semimetallic regions on GONRs film. The film becomes a mixture of semiconductive and semimetallic materials. Our observations indicate that the bandgap of GONR is very sensitive to the annealing conditions. Even at the relative mild annealing temperatures tested in this work (up to 200 °C), the ribbons contain a mixture of semiconductive and semimetallic regions. These results indicate that various processing conditions such as the baking temperature may have a dramatic effect on the bandgap and provide a possible explanation for the low bandgap (as low as 10–50 meV) observed in some GO based thin-film devices,[16] similar to that of fully annealed GONR devices (bandgap ~50 meV).[6]

ASSOCIATED CONTENT

Supporting Information

Additional XPS data, XPS fitting data, STEM images, full author list for references 15, 27, and 34. This material is available free of charge via the Internet at http://pubs.acs.org.

AUTHOR INFORMATION

Corresponding Author

rafaelv@rice.edu; tour@rice.edu

Notes

The authors declare no competing financial interest.

ACKNOWLEDGMENTS

We thank A. Ponce for his help operating the aberration-corrected STEM. The NSF PREM (DMR-0934218), AFOSR (FA9550-09-1-0581), the Lockheed Martin Corporation through the LANCER IV Program, Sandia National Laboratory, the AFRL through Universal Technology Corporation (FA8650-05-D-5807), and the ONR MURI program (#00006766, N00014-09-1-1066) for funding. R.V. acknowledges Louis and Peaches Owen for financial support.

REFERENCES

(1) Geim, A. K. *Science* **2009**, *324*, 1530.
(2) Geim, A. K.; Novoselov, K. S. *Nat. Mater.* **2007**, *6*, 183.
(3) Novoselov, K. S.; Geim, A. K.; Morozov, S. V.; Jiang, D.; Katsnelson, M. I.; Grigorieva, I. V.; Dubonos, S. V.; Firsov, A. A. *Nature* **2005**, *438*, 197.
(4) Zhang, Y. B.; Tan, Y. W.; Stormer, H. L.; Kim, P. *Nature* **2005**, *438*, 201.
(5) Li, X. L.; Wang, X. R.; Zhang, L.; Lee, S. W.; Dai, H. J. *Science* **2008**, *319*, 1229.
(6) Shimizu, T.; Haruyama, J.; Marcano, D. C.; Kosinkin, D. V.; Tour, J. M.; Hirose, K.; Suenaga, K. *Nat. Nanotechnol.* **2011**, *6*, 45.
(7) Zhu, Y.; Tour, J. M. *Nano Lett.* **2010**, *10*, 4356.
(8) Higginbotham, A. L.; Kosynkin, D. V.; Sinitskii, A.; Sun, Z. Z.; Tour, J. M. *ACS Nano* **2010**, *4*, 2059.
(9) Zhu, Y.; Higginbotham, A. L.; Tour, J. M. *Chem. Mater.* **2009**, *21*, 5284.
(10) Kosynkin, D. V.; Higginbotham, A. L.; Sinitskii, A.; Lomeda, J. R.; Dimiev, A.; Price, B. K.; Tour, J. M. *Nature* **2009**, *458*, 872.
(11) Zhu, Y.; Lu, W.; Sun, Z.; Kosynkin, D. V.; Yao, J.; Tour, J. M. *Chem. Mater.* **2011**, *23*, 935.
(12) Bai, J. W.; Duan, X. F.; Huang, Y. *Nano Lett.* **2009**, *9*, 2083.
(13) Jiao, L. Y.; Zhang, L.; Wang, X. R.; Diankov, G.; Dai, H. J. *Nature* **2009**, *458*, 877.
(14) Wang, X. R.; Dai, H. J. *Nature Chem.* **2010**, *2*, 661.
(15) Wei, Z. Q.; et al. *Science* **2010**, *328*, 1373.
(16) Eda, G.; Mattevi, C.; Yamaguchi, H.; Kim, H.; Chhowalla, M. *J. Phys. Chem. C* **2009**, *113*, 15768.
(17) Nourbakhsh, A.; Cantoro, M.; Vosch, T.; Pourtois, G.; Clemente, F.; van der Veen, M. H.; Hofkens, J.; Heyns, M. M.; De Gendt, S.; Sels, B. F. *Nanotechnology* **2010**, *21*, 435203.
(18) Yan, J. A.; Chou, M. Y. *Phys. Rev. B* **2010**, *82*, 125403.
(19) Han, M. Y.; Ozyilmaz, B.; Zhang, Y. B.; Kim, P. *Phys. Rev. Lett.* **2007**, *98*, 206805.
(20) Tseng, F.; Unluer, D.; Holcomb, K.; Stan, M. R.; Ghosh, A. W. *Appl. Phys. Lett.* **2009**, *94*, 223112 .
(21) Boukhvalov, D. W.; Katsnelson, M. I. *J. Am. Chem. Soc.* **2008**, *130*, 10697.
(22) Lahaye, R.; Jeong, H. K.; Park, C. Y.; Lee, Y. H. *Phys. Rev. B* **2009**, *79*, 125435.

(23) Sinitskii, A.; Dimiev, A.; Kosynkin, D. V.; Tour, J. M. *ACS Nano* **2010**, *4*, 5405.
(24) Zhang, Z. X.; Sun, Z. Z.; Yao, J.; Kosynkin, D. V.; Tour, J. M. *J. Am. Chem. Soc.* **2009**, *131*, 13460.
(25) Erickson, K.; Erni, R.; Lee, Z.; Alem, N.; Gannett, W.; Zettl, A. *Adv. Mater.* **2010**, *22*, 4467.
(26) Bagri, A.; Mattevi, C.; Acik, M.; Chabal, Y. J.; Chhowalla, M.; Shenoy, V. B. *Nature Chem.* **2010**, *2*, 581.
(27) Cai, W.; et al. *Science* **2008**, *321*, 1815.
(28) Liu, Z. F.; Liu, Q.; Huang, Y.; Ma, Y. F.; Yin, S. G.; Zhang, X. Y.; Sun, W.; Chen, Y. S. *Adv. Mater.* **2008**, *20*, 3924.
(29) Gross, M. L.; Hickner, M. A. *Electrochem. Solid State Lett.* **2010**, *13*, K5.
(30) Sonmez, G.; Shen, C. K. F.; Rubin, Y.; Wudl, F. *Adv. Mater.* **2005**, *17*, 897.
(31) Lerf, A.; He, H.; Forster, M.; Klinowski, J. *J. Phys. Chem. B* **1998**, *102*, 4477.
(32) Stankovich, S.; Dikin, D. A.; Piner, R. D.; Kohlhaas, K. A.; Kleinhammes, A.; Jia, Y.; Wu, Y.; Nguyen, S. T.; Ruoff, R. S. *Carbon* **2007**, *45*, 1558.
(33) Sun, Z.; Yan, Z.; Yao, J.; Beitler, E.; Zhu, Y.; Tour, J. M. *Nature* **2010**, *468*, 549.
(34) Huang, P. Y.; et al. *Nature* **2011**, *469*, 389.
(35) Mkhoyan, K. A.; Contryman, A. W.; Silcox, J.; Stewart, D. A.; Eda, G.; Mattevi, C.; Miller, S.; Chhowalla, M. *Nano Lett.* **2009**, *9*, 1058.
(36) Robertson, J.; Oreilly, E. P. *Phys. Rev. B* **1987**, *35*, 2946.